Supplement of Atmos. Chem. Phys., 21, 11655–11667, 2021
https://doi.org/10.5194/acp-21-11655-2021-supplement

Atmospheric Chemistry and Physics
Open Access

Supplement of

PM$_1$ composition and source apportionment at two sites in Delhi, India, across multiple seasons

Ernesto Reyes-Villegas et al.

Correspondence to: James Allan (james.allan@manchester.ac.uk), Gordon McFiggans (g.mcfiggans@manchester.ac.uk), and Ernesto Reyes-Villegas (ernesto.reyesvillegas@manchester.ac.uk)

Supplement of: PM$_1$ composition and source apportionment at two sites in Delhi, India across multiple seasons

S1. Monitoring sites, meteorology and dates.

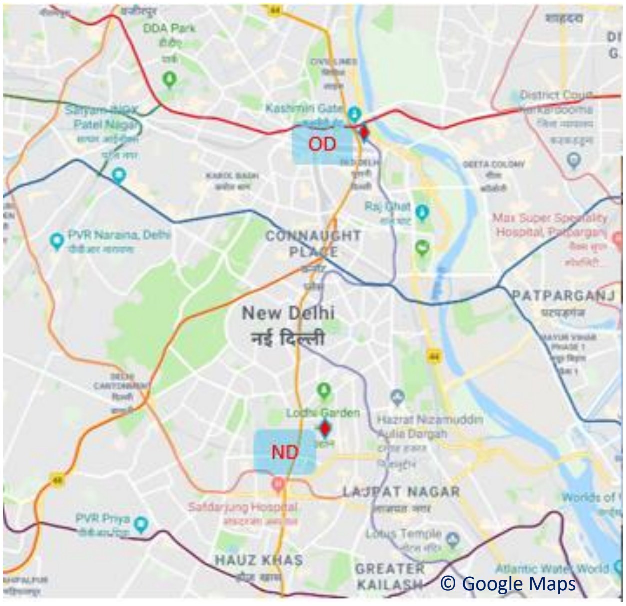

Figure S1 Location of the monitoring sites. Image taken from www.googlemaps.co.uk IGDTUW located at Old Delhi Lat 28.588°, Lon 77.217 ° and IMD located at New Delhi Lat 28.664°, Lon 77.232°.

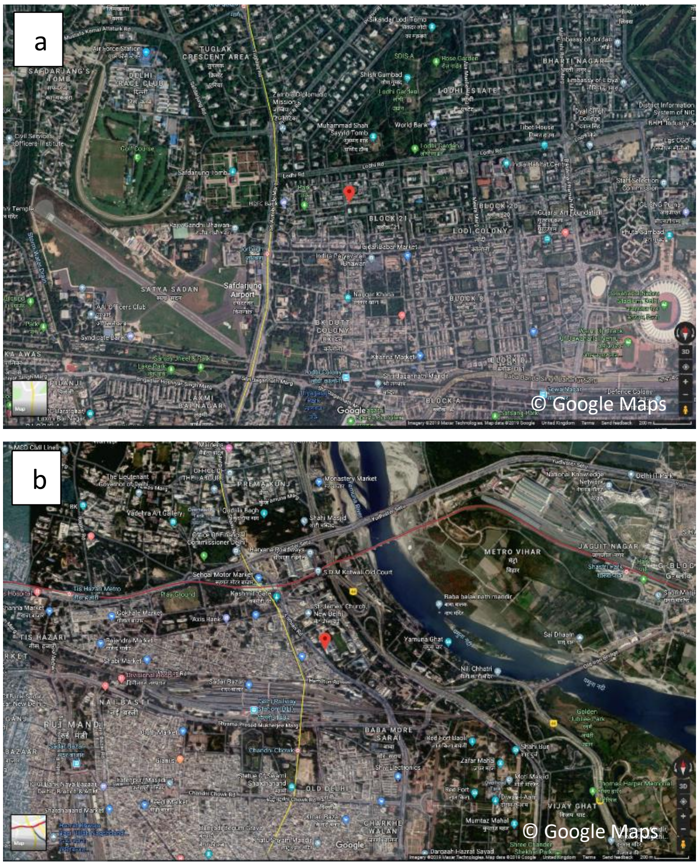

Figure S2 Maps showing the surroundings of ND (a) and OD (b). Red circle shows location of the monitoring sites.

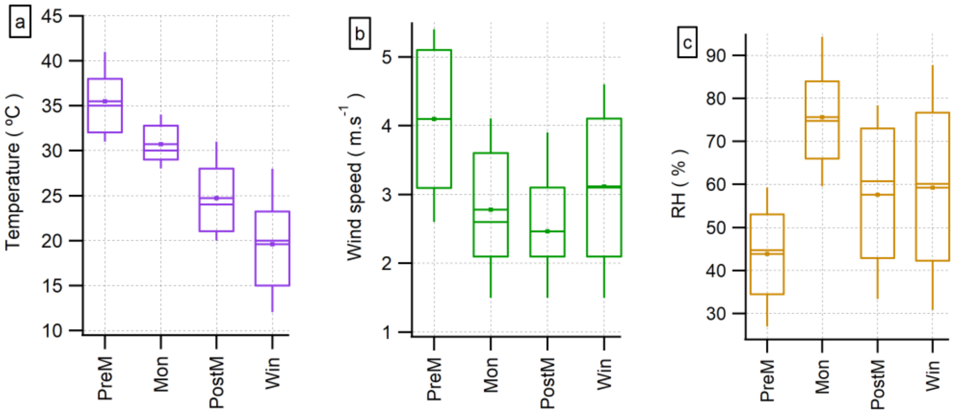

Figure S3 Box plots with temperature (a), wind speed (b) and relative humidity (c) for the different seasons. The marker represents the mean.

Table S1 Collocated instruments with the mass spectrometers.

Instrument	Event	Aditional instrumentation
ACSM	Win_ND_A	Aethalometer AE33
HR-AMS_1	PreM_ND_H1	Aethalometer AE31
cToF-AMS	PreM_OD_C	Aethalometer AE31
HR-AMS_2	PreM_OD_H2	Aethalometer AE31
HR-AMS_2	Mon_OD_H2	Aethalometer AE31
HR-AMS_2	PostM_OD_H2	Aethalometer AE31, SP2, PTR-MS, Nox, CO
cToF-AMS	PostM_OD_C	Aethalometer AE31
HR-AMS_2	PostM_OD_T_H2	Aethalometer AE31
cToF-AMS	PostM_ND_T_C	MAAP

S2. AMS quality assurance analysis. NR-PM_1 concentrations and relative contribution

S2.1 Calibrations and collection efficiency estimation.

Table S2. Nitrate ion efficiency (IE) and relative IE (RIE) for $NH4^+$, $SO4^{2-}$ and Cl^- from calibrations performed on the aerosol mass spectrometer instruments. [a]preflux period (11/10/18 - 03/11/18). [b]Diwali period (05/11/18 - 14/11/18). [c]post Diwali (14/11/18 - 23/11/18).

Instrument	Season	IE	RIE_NH_4^+	RIE_SO_4^{2-}	RIE_Cl^-	CE
cToF-AMS	PreM	1.55E-07	4.01	1.17	1.5	0.5
cToF-AMS	PostM	2.40E-07	4.6	1.2	1.7	0.5
HR-AMS_1	PreM	3.25E-07	4	1.31	1.3	0.5
HR-AMS_2	PreM	2.92E-07	4	1.45	2.07	0.5
HR-AMS_2	Mon	2.92E-07	4	1.45	2.07	0.5
HR-AMS_2	[a]PostM	2.89E-07	4	1.45	2.07	0.5
HR-AMS_2	[b]PostM	3.14E-07	4	1.45	1.05	0.8
HR-AMS_2	[c]PostM	3.14E-07	4	1.45	1.05	0.5

Collocated $PM_{2.5}$ measurements were performed in a Digitel sampler (DH-77 Digitel Enviro-sense) with a flow rate of 500 L/min. collecting 12-hour samples in quartz fibre filters. The samples were analysed with Ion Chromatography (IC) to measure anion and cation data, including blank subtraction. Components analysed include phosphate, nitrate, bromide, sulphate, nitrite, chloride, fluoride, K^+, Ca^{2+}, Mg^{2+}, $NH4^{2-}$ and Na^+. Collected filters were kept frozen and transported to the University of Birmingham for analysis. For the IC analysis, deionized water was used for blank determination and subtraction. 10 mil of DI water were added to samples. Extraction tubes were sonicated for 1 hour with bath temperature not exceeding 27 °C. Next day filter the extract solution for each sample tube using a 10 ml plastic filter and 0.45 µm syringe filter (star labs) into a new labelled polypropylene tube, finally, the sample is ready for IC analysis.

A Partisol (2025i, ThermoFisher Scientific) was deployed to perform 6-hour gravimetric $PM_{2.5}$ mass. These measurements are used in this manuscript to determine the collection efficiency of the HR-AMS_2.

For HR-AMS_2, a CE = 0.5 was used for preM and postM preflux tower periods, which was determined by comparing AMS+BC with gravimetric $PM_{2.5}$ (Fig. S4.b) and Cl^-, NO_3^- and SO_4^{2-} quantified by IC from filter measurements (Fig. S6). In the PostM flux period, for the HR-AMS_2, a CE = 1.0 was derived after comparison with total $PM_{2.5}$ (fig. S4.d). For the HR-AMS_1 measurements, a CE = 0.5 after the intercomparison with the HR-AMS_2 (fig. S7). The ACSM manual recommends using a CE = 0.5.

Figure S5 presents the time series of PM_1 online measurements (HR-AMS_2 + BC) and total gravimetric PM2.5 concentrations. Using CE = 0.5 (Fig. 5.b) shows the best agreement between PM_1 and $PM_{2.5}$, with a $PM_{2.5}$:PM_1 ratio going from 0.8 to 1.4.

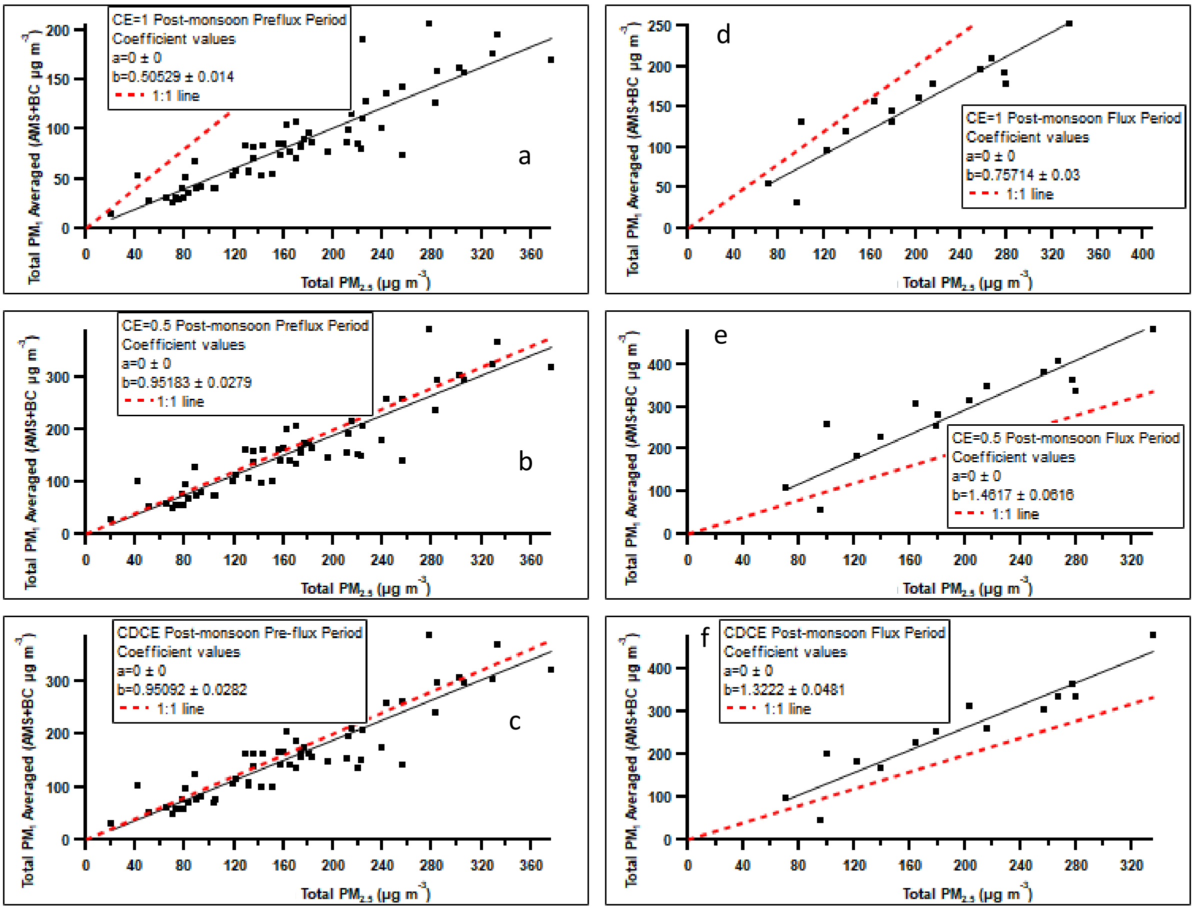

Figure S4 Comparison of total PM_1 (HR-AMS_2 + BC) with total gravimetric $PM_{2.5}$ to determine collection efficiency (CE) with HR-AMS_2 and aethalometer (BC) measurements. All AMS+BC measurements are averaged according to filter sampling times.

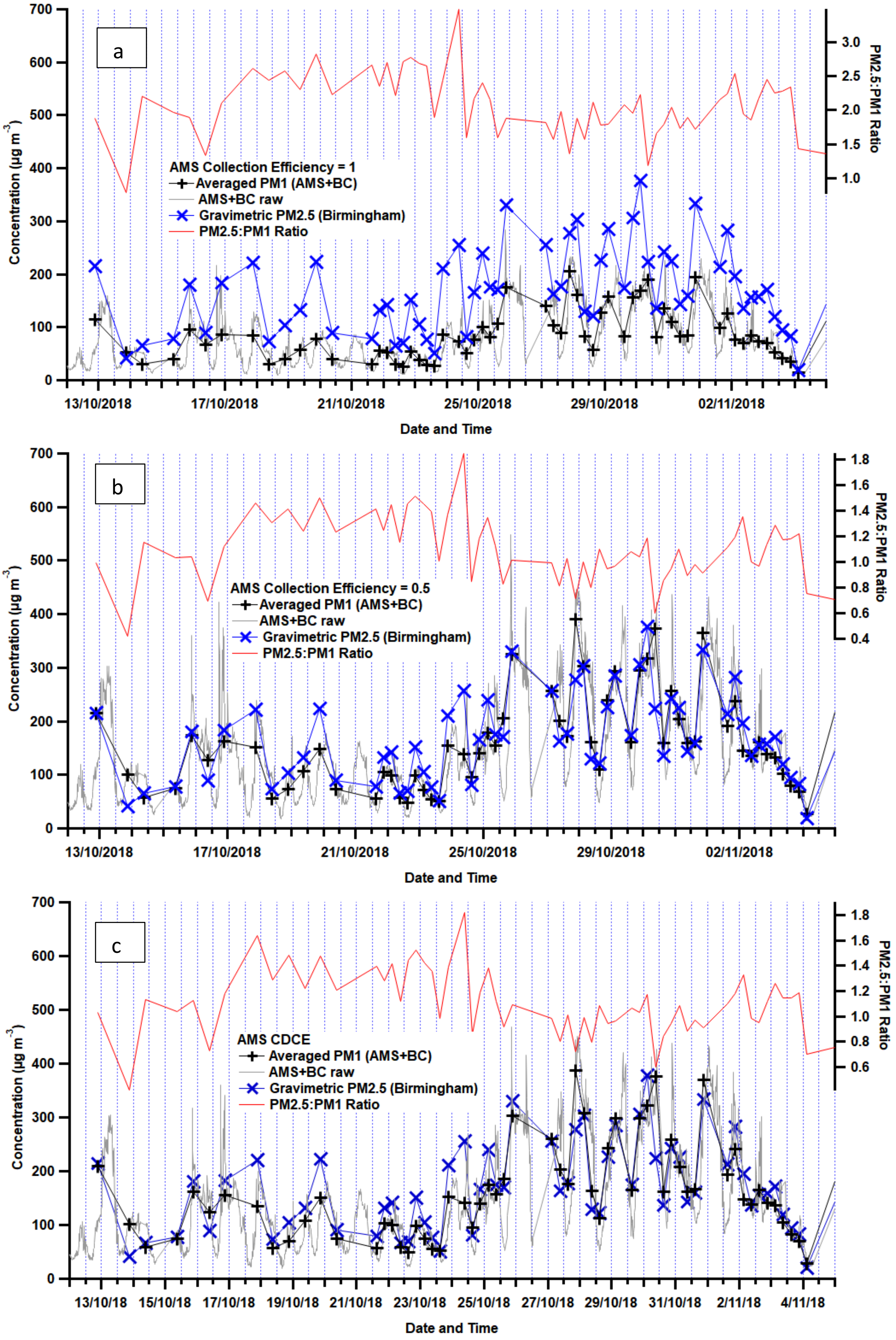

Figure S5 Analysis of the HR-AMS_2 and total gravimetric $PM_{2.5}$ for the PostMon preflux period. Time series of averaged PM_1 (AMS + BC) (black line) and gravimetric $PM_{2.5}$ (blue line) for CE =1 (a), CE = 0.5 (b) and CDCE (c). The $PM_{2.5}$:PM_1 ratio is shown in red. All AMS+BC measurements are averaged according to filter sampling times.

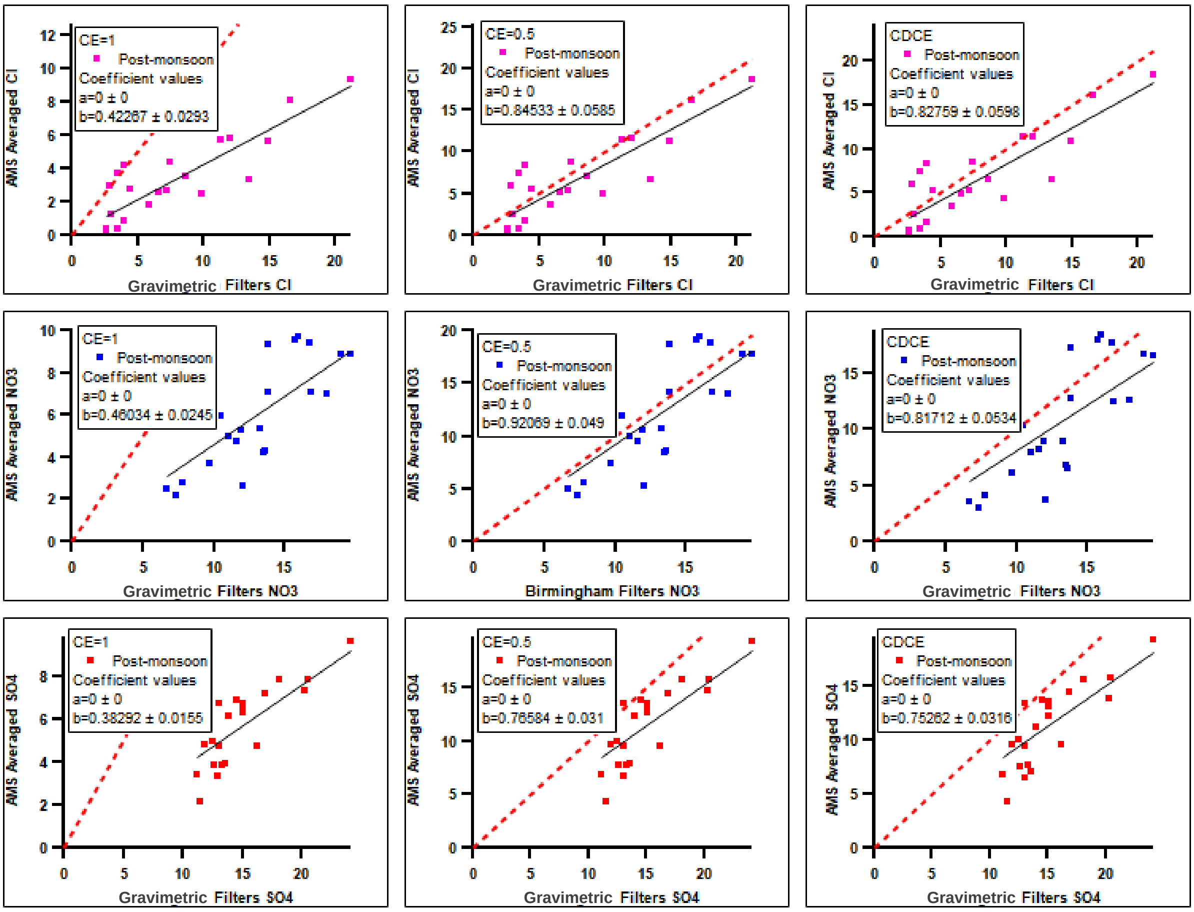

Figure S6 Correlations of Cl$^-$, NO$_3^-$ and SO$_4^{2-}$ between HR-AMS_2 and filters analysed with Ion chromatography by the University of Birmingham for CE = 1, CE = 0.5 and composition dependant CE (CDCE). All AMS+BC measurements are averaged according to filter sampling times.

S2.1 cToF-AMS and HR-AMS_2 intercomparison.

An intercomparison was performed between the cToF-AMS and the HR-ToF-AMS (fig. S7a and S7b), deployed at OD over pre-monsoon in order to perform an intercomparison (28/May – 09/June), obtaining average concentrations, in µgm^{-3}, of 15.0 and 19.1 of Org, 1.7 and 1.6 of NO$_3^-$, 6.8 and 8.3 of SO$_4^{2-}$, 2.5 and 2.6 of NH$_4^+$, 0.4 and 0.5 of Cl$^-$ for cToF-AMS and HR-ToF-AMS respectively. The total aerosol concentration for cToF-AMS is 26.5 µg.m^{-3} and for HR-ToFAMS is 32.1 µg.m^{-3}, a difference of 21%. This is well within the range of previous AMS comparison studies. Crenn et al. (2015) estimated an organic mass uncertainty of 19 %. Bahreini et al. (2009) estimated an overall uncertainty of 35 %, agreeing with other AMS studies (DeCarlo et al., 2008;Dunlea et al., 2009). Recently, a 50% uncertainty has been reported by Shinozuka et al. (2020).

A PMF analysis was performed to the Org concentrations measured by the cToF-AMS and the HR-ToF-AMS. Figure 7c shows the mass spectra comparison of the factor profiles identified and figure 7.d shows the triangle plot, f44 – f43, to compare and describe OOA. The doted lines represent the space proposed by Ng et al. (2011) to characterise OOA. The parameters f43 and f44 represent the ratio of the integrated signal at m/z 43 and m/z 44 to the total signal in the organic component mass spectrum. The same OA factors were identified in the two PMF analyses, HOA, MO-OOA, BBOA, COA and LO-

OOA. This analysis verifies the AMS intercomparison, with the same OA factors and similar ageing (f44-f43).

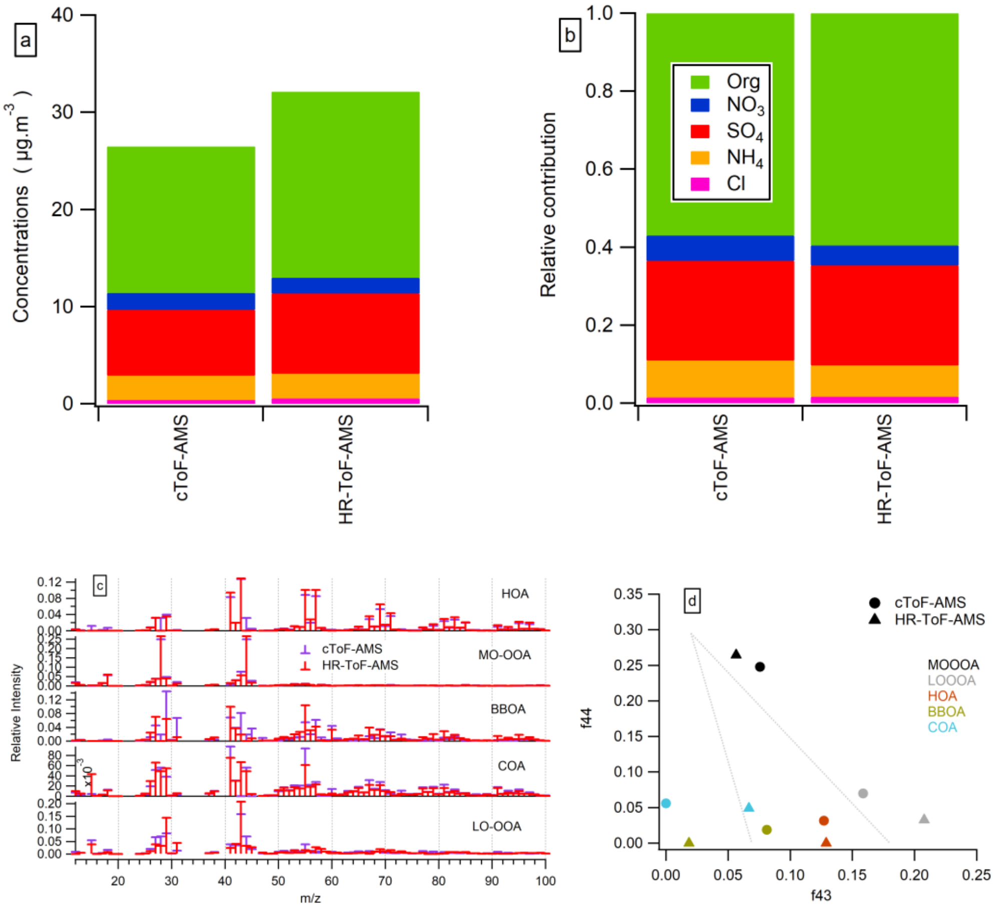

Figure S7. Average concentrations (S7.a) and relative contribution (S7.b) of Org, NO_3^-, SO_4^{2-}, NH_4^+ and Cl^- for the cToF-AMS and the HR-ToF-AMS. Mass spectra comparison from PMF analysis (S7c) and f44-f43 triangle plot (S7.d) to compare OA ageing according to Ng et al. (2011).

Table S3. Statistics of NR-PM1 and BC measurements for the various seasons. Minimum, maximum, average, standard deviation, median and number of points.

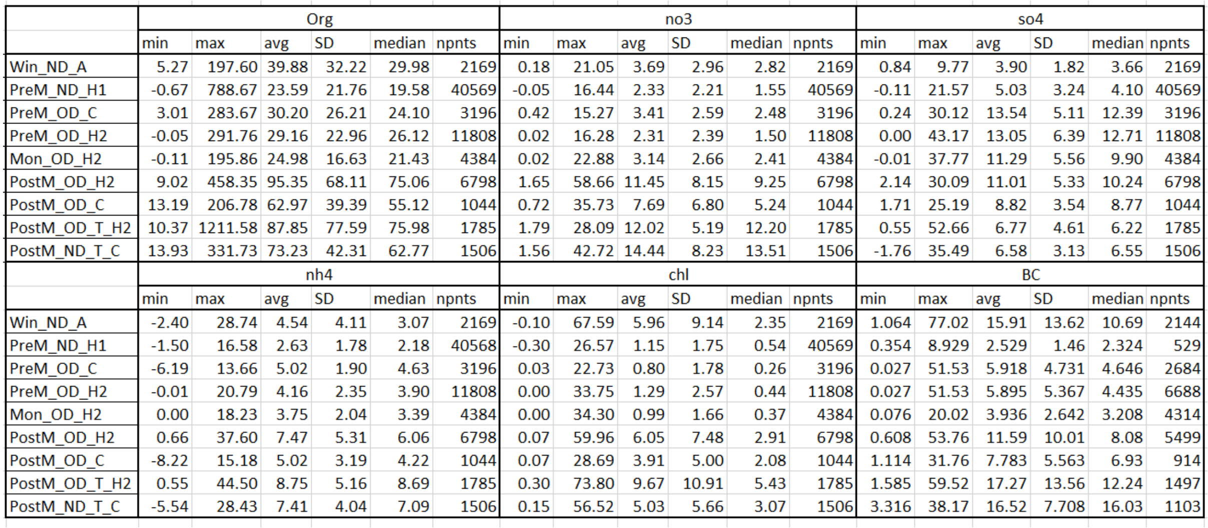

	Org						no3						so4					
	min	max	avg	SD	median	npnts	min	max	avg	SD	median	npnts	min	max	avg	SD	median	npnts
Win_ND_A	5.27	197.60	39.88	32.22	29.98	2169	0.18	21.05	3.69	2.96	2.82	2169	0.84	9.77	3.90	1.82	3.66	2169
PreM_ND_H1	-0.67	788.67	23.59	21.76	19.58	40569	-0.05	16.44	2.33	2.21	1.55	40569	-0.11	21.57	5.03	3.24	4.10	40569
PreM_OD_C	3.01	283.67	30.20	26.21	24.10	3196	0.42	15.27	3.41	2.59	2.48	3196	0.24	30.12	13.54	5.11	12.39	3196
PreM_OD_H2	-0.05	291.76	29.16	22.96	26.12	11808	0.02	16.28	2.31	2.39	1.50	11808	0.00	43.17	13.05	6.39	12.71	11808
Mon_OD_H2	-0.11	195.86	24.98	16.63	21.43	4384	0.02	22.88	3.14	2.66	2.41	4384	-0.01	37.77	11.29	5.56	9.90	4384
PostM_OD_H2	9.02	458.35	95.35	68.11	75.06	6798	1.65	58.66	11.45	8.15	9.25	6798	2.14	30.09	11.01	5.33	10.24	6798
PostM_OD_C	13.19	206.78	62.97	39.39	55.12	1044	0.72	35.73	7.69	6.80	5.24	1044	1.71	25.19	8.82	3.54	8.77	1044
PostM_OD_T_H2	10.37	1211.58	87.85	77.59	75.98	1785	1.79	28.09	12.02	5.19	12.20	1785	0.55	52.66	6.77	4.61	6.22	1785
PostM_ND_T_C	13.93	331.73	73.23	42.31	62.77	1506	1.56	42.72	14.44	8.23	13.51	1506	-1.76	35.49	6.58	3.13	6.55	1506

	nh4						chl						BC					
	min	max	avg	SD	median	npnts	min	max	avg	SD	median	npnts	min	max	avg	SD	median	npnts
Win_ND_A	-2.40	28.74	4.54	4.11	3.07	2169	-0.10	67.59	5.96	9.14	2.35	2169	1.064	77.02	15.91	13.62	10.69	2144
PreM_ND_H1	-1.50	16.58	2.63	1.78	2.18	40568	-0.30	26.57	1.15	1.75	0.54	40569	0.354	8.929	2.529	1.46	2.324	529
PreM_OD_C	-6.19	13.66	5.02	1.90	4.63	3196	0.03	22.73	0.80	1.78	0.26	3196	0.027	51.53	5.918	4.731	4.646	2684
PreM_OD_H2	-0.01	20.79	4.16	2.35	3.90	11808	0.00	33.75	1.29	2.57	0.44	11808	0.027	51.53	5.895	5.367	4.435	6688
Mon_OD_H2	0.00	18.23	3.75	2.04	3.39	4384	0.00	34.30	0.99	1.66	0.37	4384	0.076	20.02	3.936	2.642	3.208	4314
PostM_OD_H2	0.66	37.60	7.47	5.31	6.06	6798	0.07	59.96	6.05	7.48	2.91	6798	0.608	53.76	11.59	10.01	8.08	5499
PostM_OD_C	-8.22	15.18	5.02	3.19	4.22	1044	0.07	28.69	3.91	5.00	2.08	1044	1.114	31.76	7.783	5.563	6.93	914
PostM_OD_T_H2	0.55	44.50	8.75	5.16	8.69	1785	0.30	73.80	9.67	10.91	5.43	1785	1.585	59.52	17.27	13.56	12.24	1497
PostM_ND_T_C	-5.54	28.43	7.41	4.04	7.09	1506	0.15	56.52	5.03	5.66	3.07	1506	3.316	38.17	16.52	7.708	16.03	1103

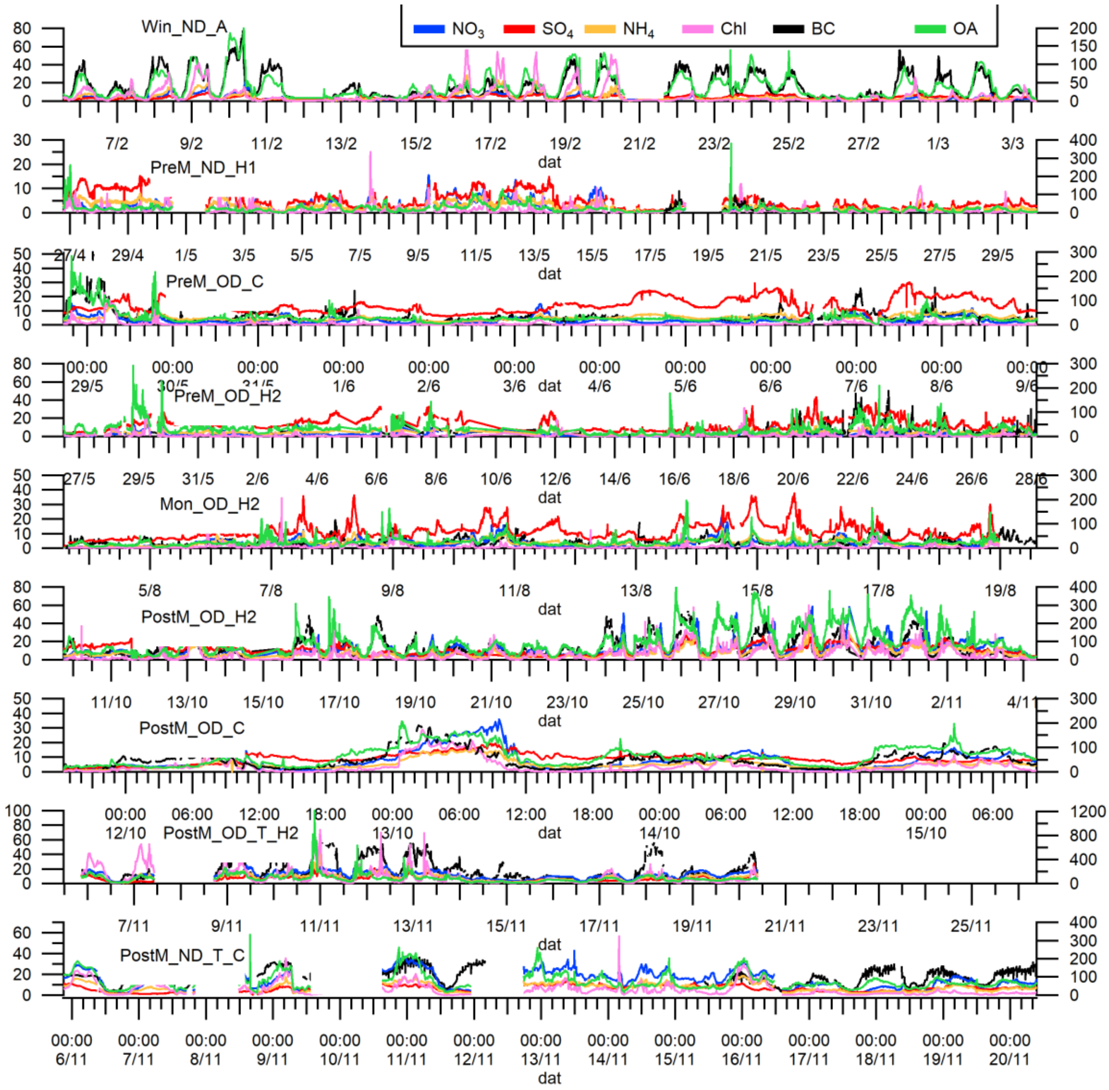

Figure S8. Aerosol time series of the various measurements. All concentrations are in µg.m^{-3}. OA concentrations are plotted on the right axis and the rest of the compounds are plotted on the left axis.

S3. PMF analysis

The selection of the optimal PMF solution was performed following recommendations in previous studies (Canonaco et al., 2013;Crippa et al., 2014;Reyes-Villegas et al., 2016) and exploring between 8-10 PMF solutions with 3, 4, 5 and 6 factors; looking at different seeds (a random starting point of the PMF solution), which resulted on analysing around 40 PMF solutions per season.

The following criteria was used to select the optimal PMF solution:

1. Residuals to be closest to zero.
2. Q/Q_{exp} value closest to one.
3. High correlation between HOA and NOx.

The PMF analysis was performed using the Source Finder (SoFi 4.8) tool (Canonaco et al., 2013) In order to select the optimal PMF solution, we analysed the overall Q/Qexp (Figure S9), the row (time series) Q/Qexp (Figure S10) and the Squares of scaled residual (Figure S11). The overall Q/Qexp is calculated as the mean of the time series Q/Qexp.

In all the PMF analyses, an improvement in the residuals and Q/Q_{exp} was observed when increasing the number of factors (Fig. S9), with Q/Qexp values of around 5.52 for 4-factor solutions and values of around 5.2 for 5-factor solutions. However, the 6-factor solutions presented two factors with similar time series and mass spectra, characteristic of factor splitting. Hence, the 5-factor solution was chosen to be further analysed.

The following figures show the PMF solution space to select the optimal PMF solution for the winter New Delhi ACSM dataset, Win_ND_A. The same analysis was performed to the other datasets to determine the optimal PMF solution for each season for further analysis presented in the manuscript.

The solutions are labelled as follows: PMF_4F_S1 is the 4-factor solution (4F) seed number one (S1). The optimal solution of this season is PMF_5F_S2. This solution showed the lowest average residuals and Q/Qexp value (Figure S9). In figure S12 the Pearson values from linear regressions between the PMF factors and NOx are displayed. NOx is a pollutant well-known to be related to traffic emissions, thus a high Pearson value is expected between HOA and NOx. High pearson values between 0.77 – 0.785 were observed with the highest Pearson value to be found with the **PMF_5F_S2** solution (0.785).

The overall Q/Qexp =5.2 is calculated as the mean of the time series Q/Qexp. The overall Q/Qexp can also be estimated from the Squares of scaled residuals. We calculate the sum of the values (Squares of scaled residual) plotted in Figure S11 for the specific PMF run. For example, for the optimal solution (PMF_5F_S2) the sum = 11269.56.

We calculate the Qexp = n * m - p*(n + m) = 147127 for the 5-factor solution, where

n = num of samples = 2169, m = num of m/z = 73, p = num of factors = 5

We also divide the Qexp by m, which gives 2015.44.

Finally, Q/Qep = 11269.56/2015.44 = 5.59, which is close to the overall Q/Qexp = 5.2.

Figures S10 and S11 are used to identify particularly high Q/Qexp values for m/z or episodes with high Q/Qexp on time series that might require further analysis. For example, we can see an episode with high Q/Qexp values on 20/20/2018 (Figure S10), which is related to an episode with high Org concentrations. Also, we can see an improvement on both time series (Figure S10) and m/z (Figure S11) plots when going from 4-factor to 5-factor solutions. However, no remarkable improvement between 5-factor solution was observed. Hence, we can use the overall Q/Qexp to select the optimal solution.

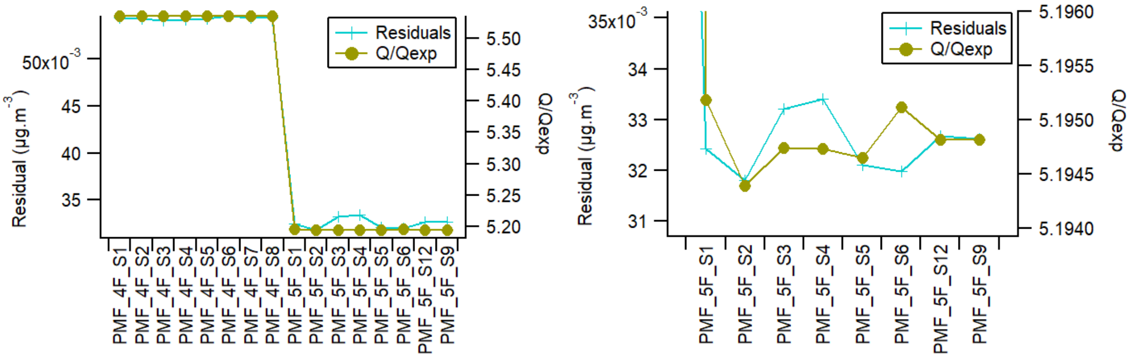

Figure S9. Summary plots of residuals and Q/Qexp values for 4 and 5 factor solutions (a) and a close up to the 5-factor solutions (b)

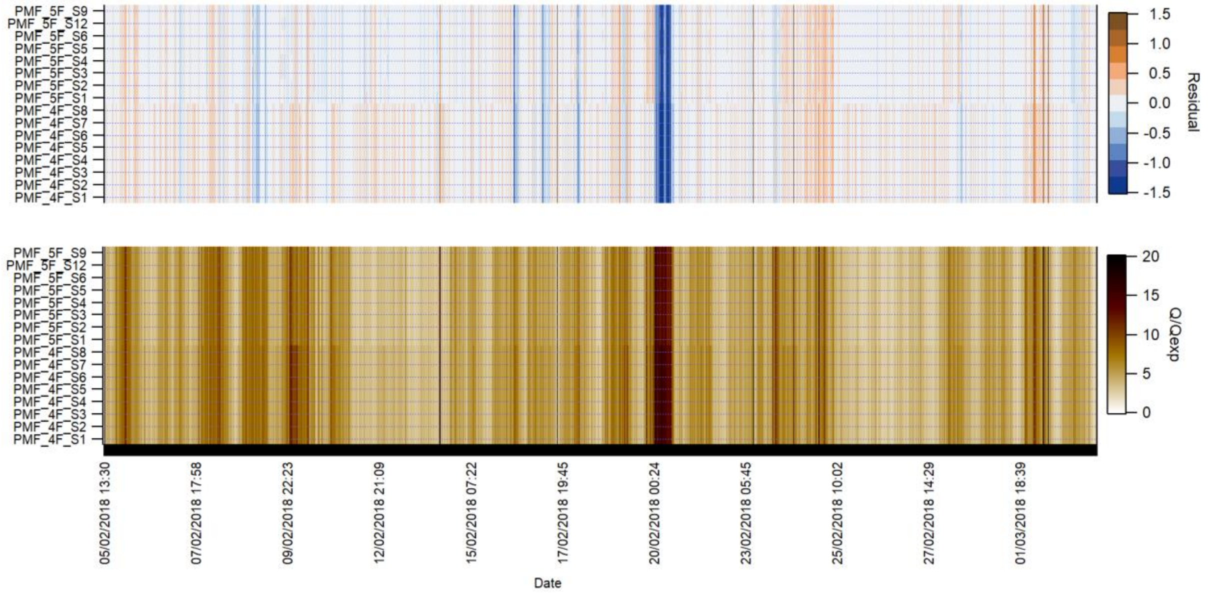

Figure S10. Time series of residuals and Q/Qexp values.

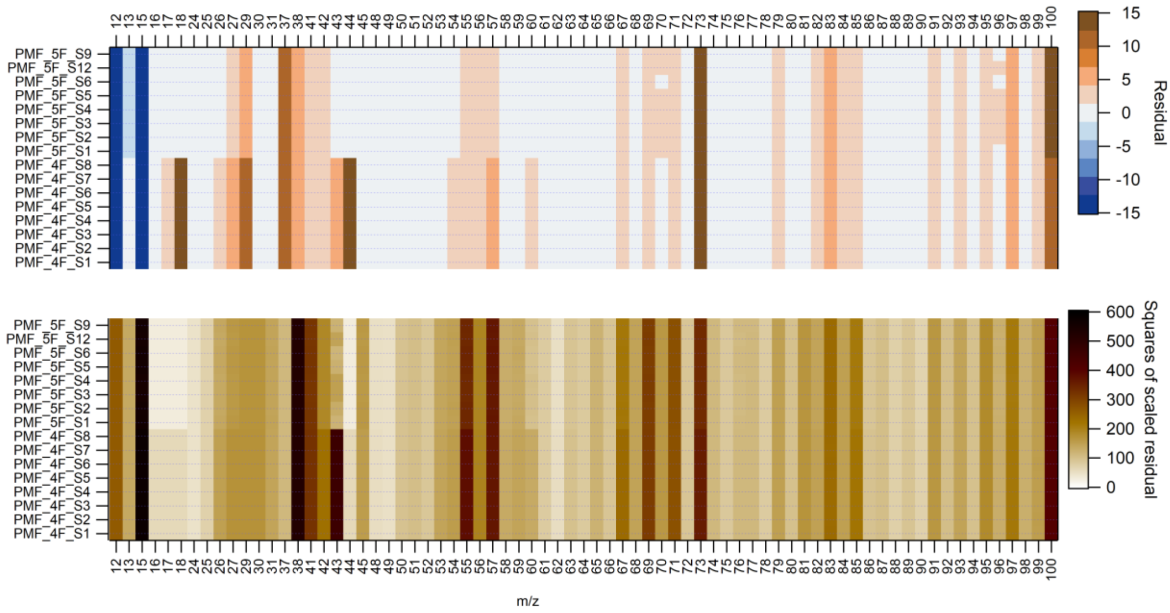

Figure S11. Residuals and Squares of scaled residual for m/z.

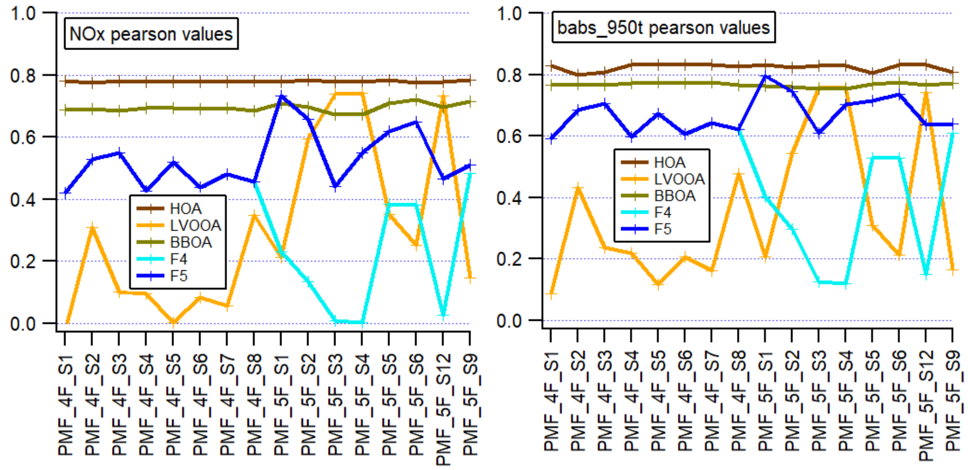

Figure S12. Pearson values of the linear regressions between the PMF factors and NOx (a) and babs_950t (b).

Table S4. Statistical parameters [µg.m^{-3}] of the PMF factors obtained from OA, measured with the HR- AMS_2, for all the various seasons. This data is analysed on detail by Cash et al. (2020), we present this data here to compare with the other PMF-AMS datasets.

		All_OD_H2		(includes PreM, Mon and PostM)									
	COA	HOA_	LVOOA	nHOA	SFOA	SVBBOA	SVOOA	HOA	BBOA	POA	SOA	TOA	POA ratio
mean	7.44	9.35	13.72	4.87	6.64	7.03	5.36	14.21	13.67	35.32	19.08	54.40	0.55
median	5.26	4.31	12.14	0.30	0.74	0.04	4.00	4.88	1.80	14.74	17.81	32.83	0.55
sd	9.55	14.30	10.89	12.65	16.05	12.81	5.85	25.71	26.45	51.35	13.21	58.69	0.21
min	0.00	0.00	0.00	0.00	0.00	0.00	0.00	0.00	0.00	0.00	0.00	0.00	0.00
max	202.87	189.56	90.90	337.90	665.03	91.39	66.84	337.90	709.60	1250.37	103.93	1250.37	1.00
		PreM_OD_H2											
	COA	HOA_	LVOOA	nHOA	SFOA	SVBBOA	SVOOA	HOA	BBOA	POA	SOA	TOA	POA ratio
mean	7.84	5.13	10.59	0.83	1.16	0.53	3.26	5.96	1.68	15.48	13.85	29.33	0.52
median	5.61	3.07	10.68	0.00	0.07	0.00	1.57	3.25	0.43	10.15	14.18	26.44	0.50
sd	8.73	6.90	7.36	2.46	3.51	1.18	4.76	8.80	3.91	17.95	9.70	23.54	0.22
min	0.00	0.00	0.00	0.00	0.00	0.00	0.00	0.00	0.00	0.00	0.00	0.00	0.00
max	131.02	118.38	53.01	30.06	75.91	12.97	56.72	136.58	84.70	233.64	61.50	290.36	1.00
		Mon_OD_H2											
	COA	HOA_	LVOOA	nHOA	SFOA	SVBBOA	SVOOA	HOA	BBOA	POA	SOA	TOA	POA ratio
mean	2.83	6.55	6.71	0.76	1.36	0.01	6.81	7.31	1.37	11.51	13.52	25.03	0.45
median	1.79	4.84	6.32	0.19	0.50	0.00	5.41	5.18	0.51	8.58	12.90	21.35	0.43
sd	3.57	5.62	5.11	1.33	3.33	0.11	5.80	6.68	3.34	11.09	8.37	16.77	0.19
min	0.00	0.00	0.00	0.00	0.00	0.00	0.00	0.00	0.00	0.00	0.00	0.00	0.01
max	41.95	59.34	35.68	14.61	60.78	3.07	66.84	67.70	60.78	130.85	66.84	197.70	1.00
		PostM_OD_H2											
	COA	HOA_	LVOOA	nHOA	SFOA	SVBBOA	SVOOA	HOA	BBOA	POA	SOA	TOA	POA ratio
mean	8.54	17.78	20.56	12.95	14.90	16.85	6.97	30.73	31.75	71.02	27.53	98.55	0.63
median	6.70	8.67	19.34	4.47	7.98	11.98	5.77	13.20	21.52	48.61	25.28	77.06	0.64
sd	7.72	21.96	11.51	17.97	18.49	15.35	5.83	39.27	30.56	64.55	13.07	69.33	0.17
min	0.00	0.00	0.00	0.00	0.00	0.00	0.00	0.00	0.00	3.25	0.00	9.05	0.24
max	101.75	189.56	90.90	119.01	186.96	91.39	44.53	281.55	247.80	456.41	103.93	460.48	1.00
		PostM_OD_T_H2											
	COA	HOA_	LVOOA	nHOA	SFOA	SVBBOA	SVOOA	HOA	BBOA	POA	SOA	TOA	POA ratio
mean	9.56	11.21	24.39	9.26	21.35	26.87	8.65	20.46	48.22	78.25	33.04	111.29	0.64
median	7.22	6.51	21.51	2.93	11.05	25.44	7.89	10.19	37.41	61.87	30.82	96.55	0.63
sd	15.55	13.09	14.51	21.27	36.38	13.00	5.53	28.83	44.79	80.12	14.63	81.24	0.14
min	0.00	0.00	0.00	0.00	0.00	1.76	0.00	0.00	2.72	5.57	0.00	14.65	0.38
max	202.87	86.99	63.69	337.90	665.03	76.43	29.20	337.90	709.60	1250.37	70.89	1250.37	1.00

POA = primary OA, SOA = secondary OA, TOA = SOA +POA. This analysis identified 7 PMF factors, we are adding HOA = HOA_ + nHOA and BBOA = SFOA + SVBBOA to compare with our 5-factor solutions in the main manuscript.

Figure S13 show the triangle plot to analyse f44 – f43 compare and describe OOA. The doted lines represent the space proposed by Ng et al. (2011) to characterise OOA. The parameters f43 and f44 represent the ratio of the integrated signal at m/z 43 and m/z 44 to the total signal in the organic component mass spectrum. We can see the typical behaviour of MOOOA with high f44 values compared to LOOOA, characteristic of a more aged, oxygenated OA. MOOOA, in black, while having different values, is found in a distinct area in the plot with f44 between 0.18 -0.26, while LOOA with low f44, 0.10 and lower, and high f43, characteristic of fresher OOA when compared with MOOOA. HOA, in brown, has a low f44, close to zero, and distinct f43 values of 0.08 - 0.13. oPOA, in purple, has slightly high values of both f44 and f43, agreeing with the identification as to be oxygenated primary organic aerosol. This analysis suggests a good separation on the oxygenated species between factor profiles and shows an f43 cluster of HOA.

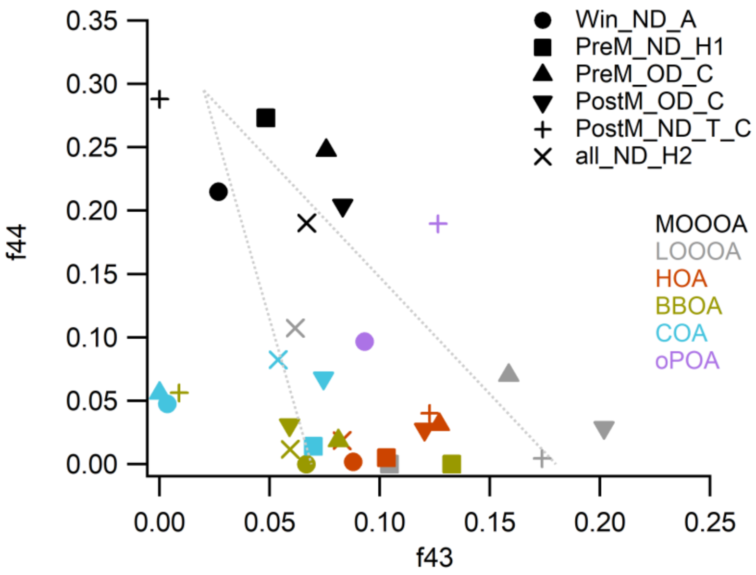

Figure S13. f44 vs f43 for all the periods and all the factor profiles and identified with PMF analysis. The symbols represent the sampling periods/sites and the colours define the PMF factor profiles.

S4. Aethalometer analysis

S4.1 Aethalometer AE-31 correction and model OD

The data collected with the aethalometer model AE-31 needs to be corrected from loading and scattering effects. The Weingarten model (Weingartner et al., 2003) has been applied using a filter loading factor f=1.30 and a multiple scattering constant C=2.8, which was calculated as the slope between BC from SP2 measurements and BC from Aethalometer after filter loading corrections. Figure S14 shows the corrected BC concentrations from the Aethalometer (red) and the BC concentrations of the SP2.

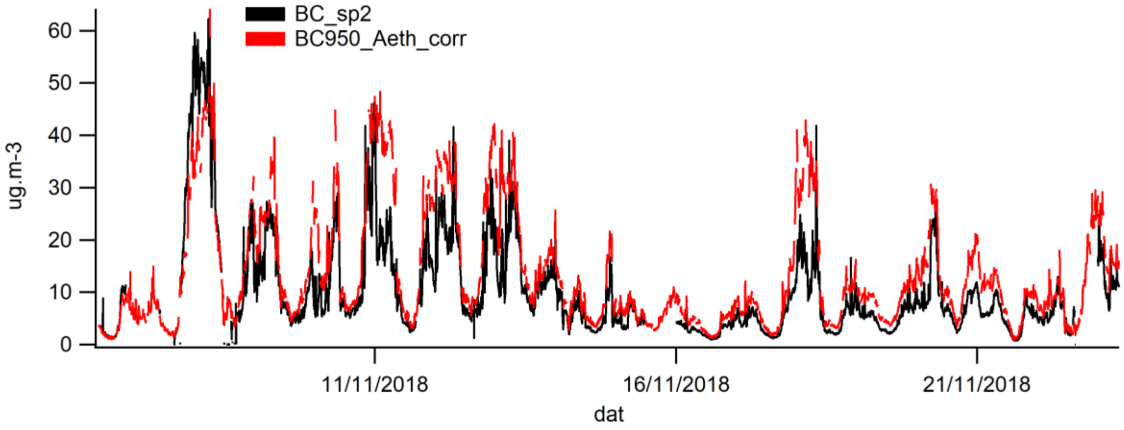

Figure S14. Intercomparison of BC measurements between aethalometer AE-31 and SP2

The aethalometer model was applied following the Sandradewi approach (Sandradewi et al., 2008) using absorption angstrom exponent traffic α_{ff} = 0.8 and wood burning α_{bb} = 2.0 (Fig. S15).

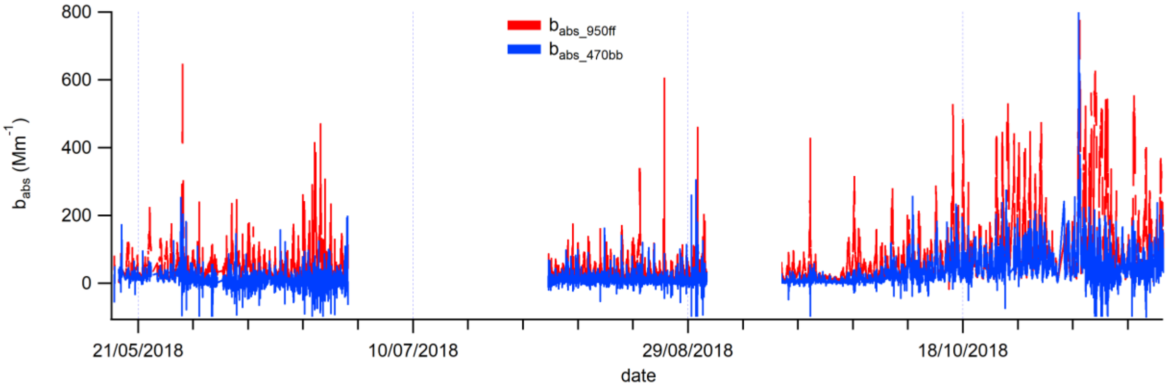

Figure S15. Aethalometer model absorption coefficients for fossil fuels (b_{abs_950ff}) and biomass burning (b_{abs_470bb}).

A sensitivity test was performed to determine α_{ff} = 0.8. and α_{bb} = 2.0, varying α_{ff} from 0.4 to 2 and α_{bb} from 1.4 to 2.6 and increments of 0.1. Figure S16 shows example plots of the performed analysis. An improvement was observed when using α_{ff} of 0.8 compared to 1.0, thus a value of 0.8 was derived (figures S16.a and S16.b). No significant changes were observed when testing different α_{bb} values (figures S16.c and S16.d), thus the default value of 2.0 was used (Fig. S16). A similar analysis was performed to select values for the subsequent Aethalometer model analyses.

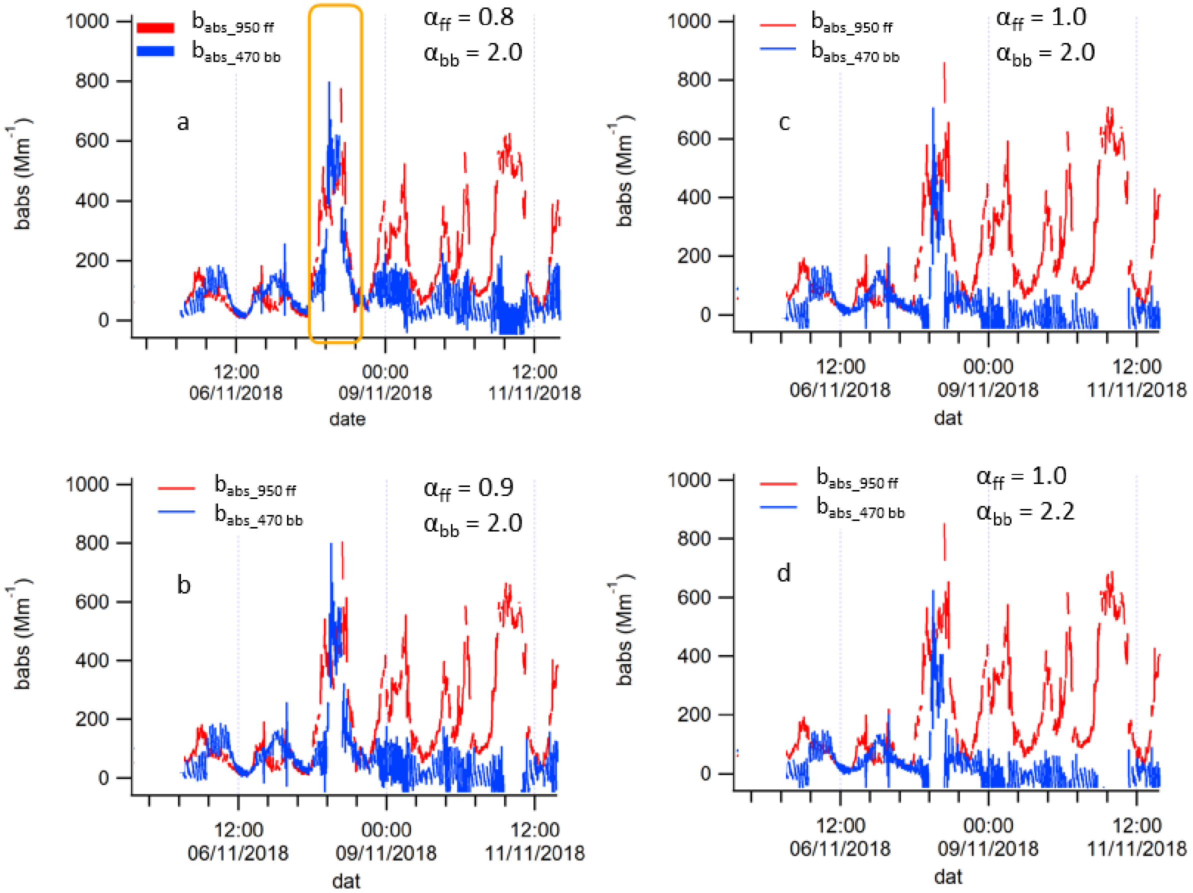

Figure S16. Sensitivity test to select α_{ff} = 0.8. The peak marked in panel (a) relates to the Diwali celebrations.

S4.2 Aethalometer model outputs AE-31 PreM_ND.

The aethalometer model was applied following the Sandradewi approach (Sandradewi et al., 2008) using an absorption angstrom exponent for fossil fuel of α_{ff} = 0.8 and for biomass burning of α_{bb} = 2.0 (Fig. S17), after doing a sensitivity test.

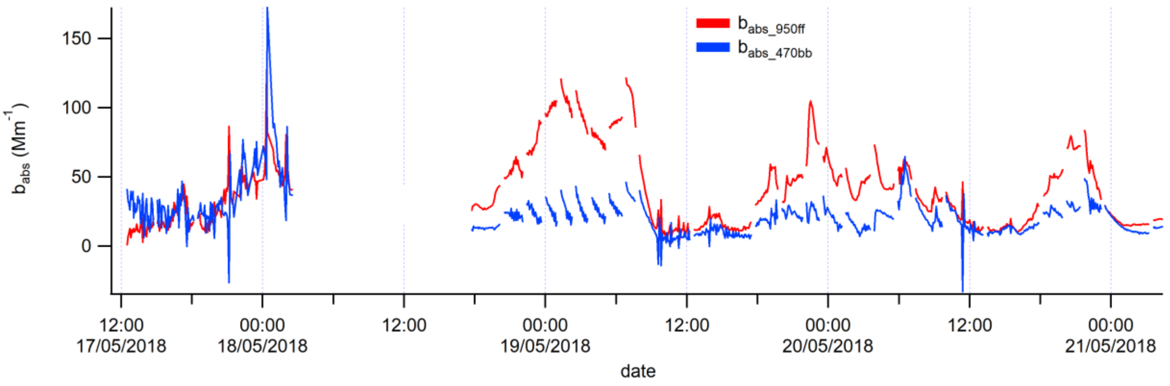

Figure S17. Aethalometer model absorption coefficients for traffic ($b_{abs\_950\ ff}$) and wood burning ($b_{abs\_470\ bb}$).

S4.3 Aethalometer model outputs AE-33 ND-Winter.

The aethalometer model was applied following the Sandradewi approach (Sandradewi et al., 2008) using absorption angstrom exponent fossil fuel α_{ff} = 1.0 and biomass burning α_{bb} = 2.0 (Fig. S18), after doing a sensitivity test.

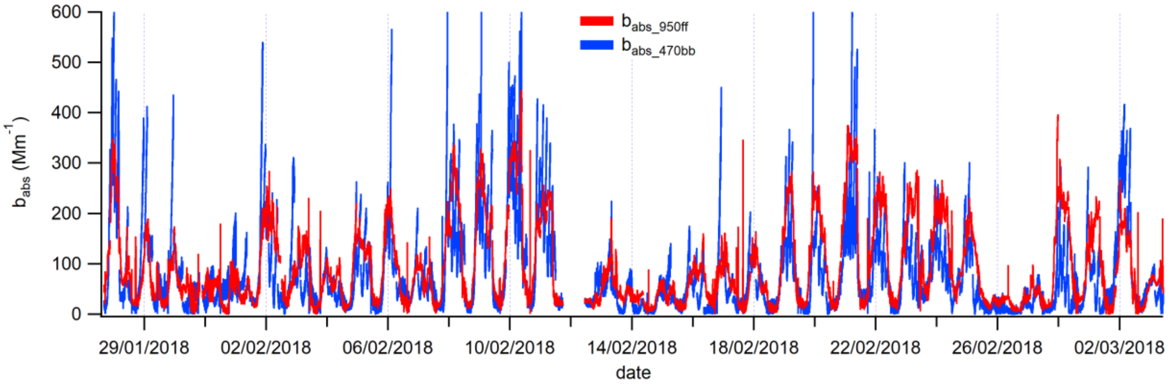

Figure S18. Aethalometer model applied to AE-33 model in Winter.

S5. Analysis of wind speed and direction.

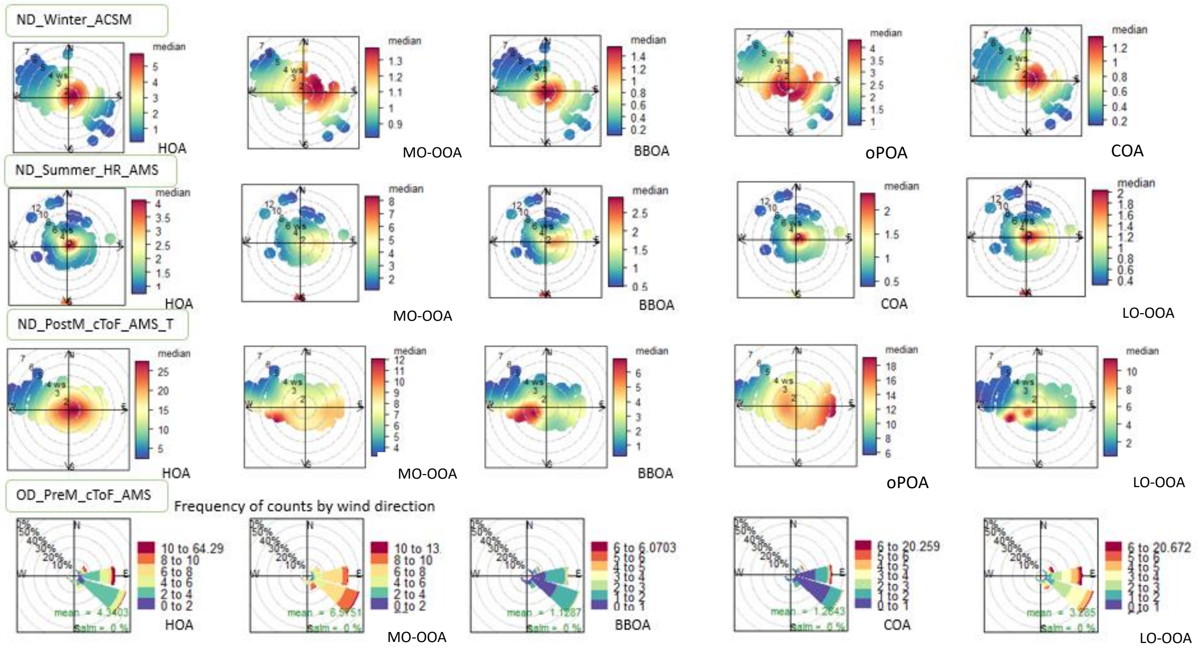

Figure S19. Polar plots of OA factors median concentrations [µg.m^{-3}]. Due to the low number of data points for OD_PreM_cToF_AMS to plot polar plots, pollution roses are presented.

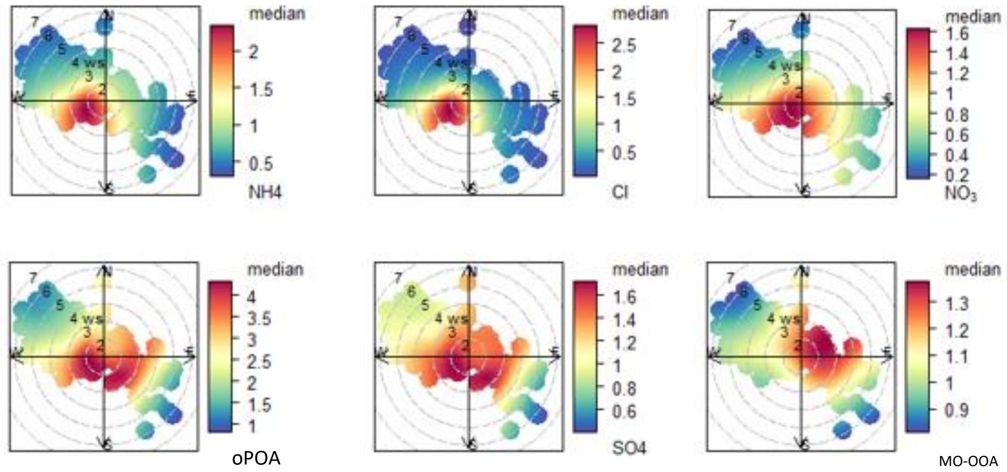

Figure S20. Polar plots of various aerosols. Median concentrations [µg.m^{-3}].

References

Bahreini, R., Ervens, B., Middlebrook, A. M., Warneke, C., de Gouw, J. A., DeCarlo, P. F., Jimenez, J. L., Brock, C. A., Neuman, J. A., Ryerson, T. B., Stark, H., Atlas, E., Brioude, J., Fried, A., Holloway, J. S., Peischl, J., Richter, D., Walega, J., Weibring, P., Wollny, A. G., and Fehsenfeld, F. C.: Organic aerosol formation in urban and industrial plumes near Houston and Dallas, Texas, Journal of Geophysical Research: Atmospheres, 114, https://doi.org/10.1029/2008JD011493, 2009.

Canonaco, F., Crippa, M., Slowik, J. G., Baltensperger, U., and Prevot, A. S. H.: SoFi, an IGOR-based interface for the efficient use of the generalized multilinear engine (ME-2) for the source apportionment: ME-2 application to aerosol mass spectrometer data, Atmos Meas Tech, 6, 3649-3661, DOI 10.5194/amt-6-3649-2013, 2013.

Cash, M. J., Langford, B., Di Marco, C., Mullinger, N., Allan, J., Reyes-Villegas, E., Ruthambara, J., Heal, M., Acton, W., F. J., Drysdale, W., Tuhin, M., Shivani, Ranu, G., and Nemitz, E.: Seasonal analysis of submicron aerosol in Old Delhi using high resolution aerosol mass spectrometry: Chemical characterisation, source apportionment and new marker identification, In-preparation, 2020.

Crenn, V., Sciare, J., Croteau, P. L., Verlhac, S., Fröhlich, R., Belis, C. A., Aas, W., Äijälä, M., Alastuey, A., Artiñano, B., Baisnée, D., Bonnaire, N., Bressi, M., Canagaratna, M., Canonaco, F., Carbone, C., Cavalli, F., Coz, E., Cubison, M. J., Esser-Gietl, J. K., Green, D. C., Gros, V., Heikkinen, L., Herrmann, H., Lunder, C., Minguillón, M. C., Močnik, G., O'Dowd, C. D., Ovadnevaite, J., Petit, J. E., Petralia, E., Poulain, L., Priestman, M., Riffault, V., Ripoll, A., Sarda-Estève, R., Slowik, J. G., Setyan, A., Wiedensohler, A., Baltensperger, U., Prévôt, A. S. H., Jayne, J. T., and Favez, O.: ACTRIS ACSM intercomparison – Part 1: Reproducibility of concentration and fragment results from 13 individual Quadrupole Aerosol Chemical Speciation Monitors (Q-ACSM) and consistency with co-located instruments, Atmos. Meas. Tech., 8, 5063-5087, 10.5194/amt-8-5063-2015, 2015.

Crippa, M., Canonaco, F., Lanz, V. A., Aijala, M., Allan, J. D., Carbone, S., Capes, G., Ceburnis, D., Dall'Osto, M., Day, D. A., DeCarlo, P. F., Ehn, M., Eriksson, A., Freney, E., Ruiz, L. H., Hillamo, R., Jimenez, J. L., Junninen, H., Kiendler-Scharr, A., Kortelainen, A. M., Kulmala, M., Laaksonen, A., Mensah, A., Mohr, C., Nemitz, E., O'Dowd, C., Ovadnevaite, J., Pandis, S. N., Petaja, T., Poulain, L., Saarikoski, S., Sellegri, K., Swietlicki, E., Tiitta, P., Worsnop, D. R., Baltensperger, U., and Prevot, A. S. H.: Organic aerosol components derived from 25 AMS data sets across Europe using a consistent ME-2 based source apportionment approach, Atmos Chem Phys, 14, 6159-6176, DOI 10.5194/acp-14-6159-2014, 2014.

DeCarlo, P. F., Dunlea, E. J., Kimmel, J. R., Aiken, A. C., Sueper, D., Crounse, J., Wennberg, P. O., Emmons, L., Shinozuka, Y., Clarke, A., Zhou, J., Tomlinson, J., Collins, D. R., Knapp, D., Weinheimer, A.

J., Montzka, D. D., Campos, T., and Jimenez, J. L.: Fast airborne aerosol size and chemistry measurements above Mexico City and Central Mexico during the MILAGRO campaign, Atmos Chem Phys, 8, 4027-4048, 2008.

Dunlea, E. J., DeCarlo, P. F., Aiken, A. C., Kimmel, J. R., Peltier, R. E., Weber, R. J., Tomlinson, J., Collins, D. R., Shinozuka, Y., McNaughton, C. S., Howell, S. G., Clarke, A. D., Emmons, L. K., Apel, E. C., Pfister, G. G., van Donkelaar, A., Martin, R. V., Millet, D. B., Heald, C. L., and Jimenez, J. L.: Evolution of Asian aerosols during transpacific transport in INTEX-B, Atmos. Chem. Phys., 9, 7257-7287, 10.5194/acp-9-7257-2009, 2009.

Ng, N., Canagaratna, M., Jimenez, J., Chhabra, P., Seinfeld, J., and Worsnop, D.: Changes in organic aerosol composition with aging inferred from aerosol mass spectra, Atmos Chem Phys, 11, 6465-6474, 2011.

Reyes-Villegas, E., Green, D. C., Priestman, M., Canonaco, F., Coe, H., Prévôt, A. S. H., and Allan, J. D.: Organic aerosol source apportionment in London 2013 with ME-2: exploring the solution space with annual and seasonal analysis, Atmos. Chem. Phys., 16, 15545-15559, 10.5194/acp-16-15545-2016, 2016.

Sandradewi, J., Prévôt, A. S. H., Szidat, S., Perron, N., Alfarra, M. R., Lanz, V. A., Weingartner, E., and Baltensperger, U. R. S.: Using aerosol light abosrption measurements for the quantitative determination of wood burning and traffic emission contribution to particulate matter, Environmental Science and Technology, 42, 3316-3323, 10.1021/es702253m, 2008.

Shinozuka, Y., Saide, P. E., Ferrada, G. A., Burton, S. P., Ferrare, R., Doherty, S. J., Gordon, H., Longo, K., Mallet, M., Feng, Y., Wang, Q., Cheng, Y., Dobracki, A., Freitag, S., Howell, S. G., LeBlanc, S., Flynn, C., Segal-Rosenhaimer, M., Pistone, K., Podolske, J. R., Stith, E. J., Bennett, J. R., Carmichael, G. R., da Silva, A., Govindaraju, R., Leung, R., Zhang, Y., Pfister, L., Ryoo, J. M., Redemann, J., Wood, R., and Zuidema, P.: Modeling the smoky troposphere of the southeast Atlantic: a comparison to ORACLES airborne observations from September of 2016, Atmos. Chem. Phys., 20, 11491-11526, 10.5194/acp-20-11491-2020, 2020.

Weingartner, E., Saathoff, H., Schnaiter, M., Streit, N., Bitnar, B., and Baltensperger, U.: Absorption of light by soot particles: determination of the absorption coefficient by means of aethalometers, J Aerosol Sci, 34, 1445-1463, 10.1016/S0021-8502(03)00359-8, 2003.